Development of a Flying Robot with Pantograph-based Variable Wing Mechanism

Naohiro Hara, Kazuo Tanaka, *Member, IEEE,* Hiroshi Ohtake, *Member, IEEE,* and Hua O. Wang, *Senior Member, IEEE*

***Abstract*— We develop a flying robot with a new pantograph-based variable wing mechanism for horizontal-axis rotorcrafts (cyclogyro rotorcrafts). A key feature of the new mechanism is to have a unique trajectory of variable wings that not only change angles of attack but also expand and contract according to wing positions. As a first step, this paper focuses on demonstrating the possibility of the flying robot with this mechanism. After addressing the pantograph-based variable wing mechanism and its features, a simulation model of this mechanism is constructed. Next, we present some comparison results (between the simulation model and experimental data) for a prototype body with the proposed pantograph-based variable wing mechanism. Both simulation and experimental results show that the flying robot with this new mechanism can generate enough lift forces to keep itself in the air. Furthermore, we construct a more precise simulation model by considering rotational motion of each wing. As a result of optimizing design parameters using the precise simulation model, flight performance experimental results demonstrate that the robot with the optimal design parameters can generate not only enough lift forces but also 155 gf payload.**

***Index Terms*— Flying robot, pantograph-based variable wing mechanism, horizontal-axis rotorcrafts, optimal design.**

I. INTRODUCTION

THERE have been a number of studies on flying machines in the last few decades. Most of studies on airplanes and gliders as fixed wing aircrafts, helicopters as vertical-axis rotorcrafts, and balloons as lighter-than-air aircrafts have focused on improving their flying performance rather than on developing new and innovative flying mechanisms.

In recent years, flying robotics researches [1] - [7] have been mainly conducted from the biologically inspired points of view. Another recent topic on flying robots is micro air vehicles (MAVs), e.g., [8]. In particular, the DARPA project (e.g., [9], [10]) on MAVs is well known. Although a number of MAV studies have been reported in the literature, e.g., [11–14], there are few studies on small-size horizontal-axis rotorcrafts. This paper deals with development of a small-size horizontal-axis rotorcraft mechanism that is different from that used in [1] - [14].

Manuscript received January 20, 2002; revised November 18, 2002. This work was supported in part by a Grant-in-Aid for Scientific Research (C) 18560244 from the Ministry of Education, Science and Culture of Japan.

Naohiro Hara, Kazuo Tanaka and Hiroshi Ohtake are with the Department of Mechanical Engineering and Intelligent Systems, The University of Electro-Communications, Chofu, Tokyo 182-8585 Japan (email: n-hara@rc.mce.uec.ac.jp; ktanaka@mce.uec.ac.jp; hohtake@rc.mce.uec.ac.jp).

Hua O. Wang is with the Department of Aerospace and Mechanical Engineering, Boston University, Boston, MA 02215 USA (email: wangh@bu.edu).

Very recently, a new and innovative mechanism for very few types of horizontal-axis rotorcrafts has been proposed in [15] [16] [17]. The horizontal-axis rotorcrafts are called ”cyclogyro”. Cyclogyro that is a unique mechanism of generating lift forces was proposed in 1930’s. The cyclogyro is a rotorcraft propelled and given lift by horizontal assemblies of rotating wings. Very few prototypes were built, and those that were constructed were completely unsuccessful. The essential principle is that the angle of attack of the rotating wings is altered as they go round, allowing the lift/thrust vector to be altered. This allows the rotorcraft to rise vertically, hover, and even go backwards. Thus, cyclogyro-based flying robot has possibility of being a high maneuverability MAV. However, to the best of our knowledge, nobody has proposed effective and practical mechanisms of altering angles of attack until the mechanism [17] has been proposed. This is the main reason that there has been no record of any successful flights although rotorcrafts of this type have been designed by some companies. Very recently, it was shown in [17] that the developed cyclogyro-based flying robot can generate at least enough lift force to fly. However, in spite of the successful development of the cyclogyro-based flying robot, its payload was very few (only about 10 g). Hence, we need to develop a flying robot that realizes more efficient flight performance.

The main purpose of this paper is to develop a more efficient and innovative flying mechanism for cyclogyro-based horizontal axis rotorcrafts. To accomplish the purpose, in this paper, we newly propose a pantograph-based variable wing mechanism that can be regarded as an extension of that proposed in [17]. A key feature of the new mechanism is to have a unique trajectory of variable wings that not only change angles of attack but also expand and contract according to wing positions. As a first step, this paper focuses on demonstrating the possibility of the flying robot with this mechanism.

The rest of the paper is organized as follows. Section II describes a pantograph-based variable wing mechanism and its features. In Section III, we construct a simulation model of this mechanism and present some comparison results (between the simulation model and experimental data) for a prototype body with the mechanism. Both simulation and experimental results show that the flying robot with the mechanism can generate enough lift forces to keep itself in the air. Furthermore, we construct a more precise simulation model by considering rotational motion in Section IV. Section V gives design parameters optimization using the precise simulation model. As a result of optimizing design parameters using the precise simulation

model, flight performance experimental results demonstrate that the robot with the optimal design parameters can generate not only enough lift forces but also 155 gf payload.

II. Pantograph-based Variable Wing Mechanism

Fig. 1 illustrates an outline of our robot with the pantograph-based variable wing mechanism proposed in this paper. The robot consists of three pantograph-based variable wing units. Each unit has two wing segments. As will be mentioned later, the numbers of pantograph-based variable wing units and wing segments are design parameters of the robot. This mechanism is composed of two different mechanisms. One is a revolving slider-crank mechanism that causes revolving and reciprocating motion. The other is a pantograph-link mechanism that causes flapping motion.

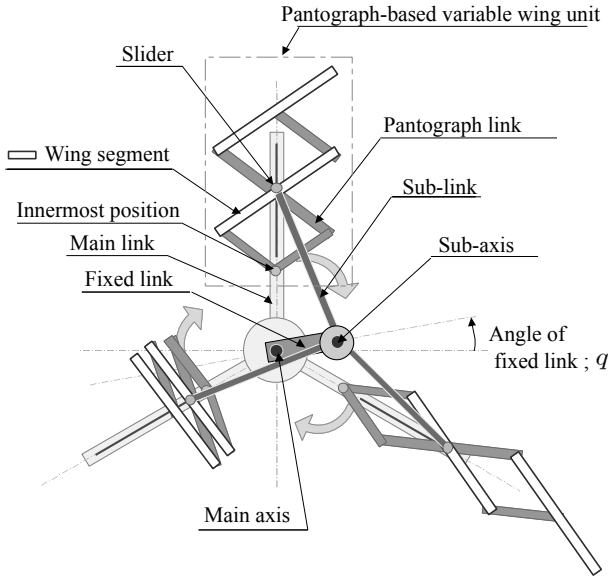

Fig. 1. Outline of robot with three pantograph-based variable wing units.

As the main links rotate around the main axis, the sub-links also rotate around the sub-axis due to the slider-crank mechanism. The innermost position of a pantograph-based variable wing unit is connected to the main link and the first segment is linked to the slider that is connected on the end of the sub-link. Thus the pantograph links expand and contract, as the sliders shuttle along the linear guides on the main link. Because of these motions, the wing segments (located on the pantograph links like as in Fig. 1) reciprocate and swing around the center of the wing chord.

Fig. 2 shows the trajectory of the wing segments according to the revolution of the main link. In downstroke motion of the wing segments, this mechanism can generate heavy drags (, i.e., lift forces) to the upward direction by expanding the wings with larger angles of attack. Conversely in upstroke motion, this mechanism can reduce anti-lift forces to the downward direction by contracting the wings with smaller angles of attack. Due to this folding up motion of the wings, it is possible for this mechanism to have a larger wing area in a small space and to get a larger lift force in comparison with the mechanism proposed in [17].

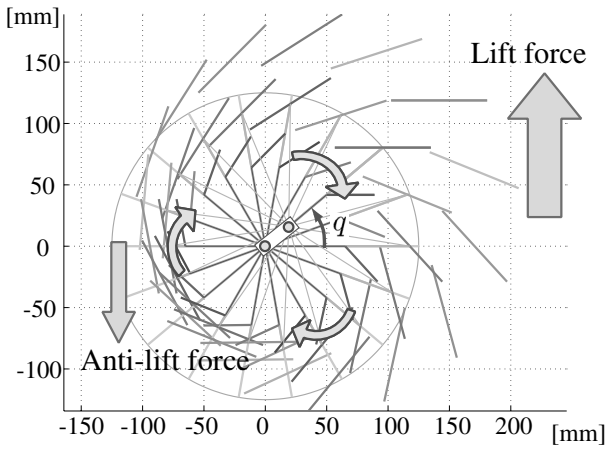

Fig. 2. Trajectory of variable wings.

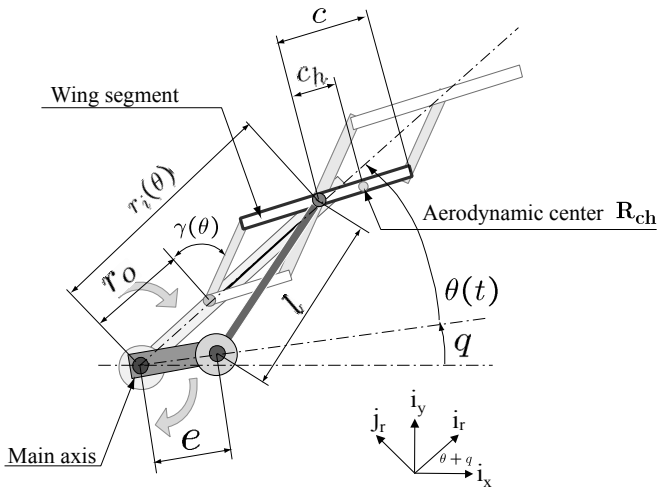

Fig. 3. Design parameters and variables in a pantograph-based variable wing unit.

The symbols and variables in this paper are summarized in Fig. 3. The parameters of the robot used in this paper are listed below.

l:length of sub-links,
e:length of fixed link,
c:length of pantograph links,
b:length of wing spans,
q:angle of fixed link,
θ:rotating angle of main link,
n_f:number of pantograph-based variable wing units,
n:number of wing segments,
r_0:radius of first pantograph segment,
$r_i(\theta)$:radius of wing segment i,
$\gamma(\theta)$:flapping angle of wing segments.

Fig. 4 shows the developed prototype body with the proposed mechanism. The design parameters of the developed prototype body (245 g) are as follows:

$l = 100$ [mm], $e = 25$ [mm],$c = 40$ [mm],
$b = 230$ [mm], $n_f = 5$ [units], $n = 2$ [seg.].

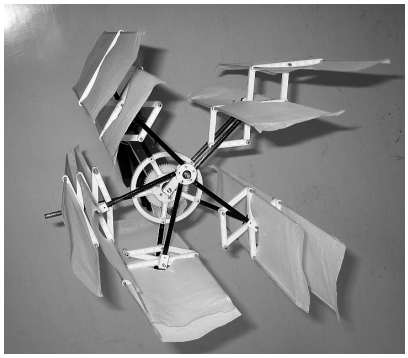

Fig. 4. Developed prototype body with five pantograph-based variable wing units.

The prototype body has five sets ($n_f = 5$) of variable wings with two wing segments ($n = 2$), and is totally 245 g including a brushless DC motor.

III. Simulation model

This section presents a simulation model for calculating lift force and power of the proposed mechanism and shows the possibility of flying the robot through the developed simulation model and experiments.

A. Trajectories of Wing Segments

In the mechanism, the radius $r_i(\theta)$ of the wing segment i and the wing's flapping angle $\gamma(\theta)$ are functions of rotating angle $\theta(t)$ of the main axis as shown in Fig 3:

$$r_i(\theta) = r_o + (r_m(\theta) - r_o)i, \quad (1)$$

$$\gamma(\theta) = cos^{-1}\frac{r_m(\theta) - r_o}{2l}, \quad (2)$$

where $r_m(\theta) = e\,cos\theta + \sqrt{l^2 - e^2 sin^2(\theta)}$. The vector $\mathbf{R}_{ch}(\theta)$ from the main axis to the aerodynamic center on the wing chord (see Fig. 3) is expressed as

$$\begin{aligned}\mathbf{R}_{ch}(\theta) &= (r_i(\theta) + c_h sin\gamma)\mathbf{i}_r - c_h cos\gamma \mathbf{j}_r \\ &= \begin{bmatrix} r_i(\theta) + c_h sin\gamma \\ c_h cos\gamma \end{bmatrix}^T \\ &\times \begin{bmatrix} cos(\theta+q) & sin(\theta+q) \\ -sin(\theta+q) & cos(\theta+q) \end{bmatrix} \begin{bmatrix} \mathbf{i}_x \\ \mathbf{i}_y \end{bmatrix}. \quad (3)\end{aligned}$$

B. Translational Lift

The simulation model discussed in Section III simply considers only translational motions of the wings in the mechanism, as illustrated in Fig. 5. To consider the translation of wing segments based on the quasi-steady theory, we need to obtain the translating velocity v^* that gives an average of dynamical pressure. In this paper, for simplicity, we fix the aerodynamic center at the 1/4 chord position $\mathbf{R}_{ch}(c_h = c/2)$. Hence for a rotational frequency $f[Hz]$ of the main link, the translating velocity of the wing segment i is calculated as

$$v_i^*(\theta) = |\mathbf{v}_i^*| \cong \frac{2\pi f}{\delta\theta}\sqrt{\Delta R_{c_h x_i}^2(\theta) + \Delta R_{c_h y_i}^2(\theta)}, \quad (4)$$

$$\phi_i(\theta) = \angle \mathbf{v}_i^* \cong \frac{\Delta R_{c_h y_i}(\theta)}{\Delta R_{c_h x_i}(\theta)}, \quad (5)$$

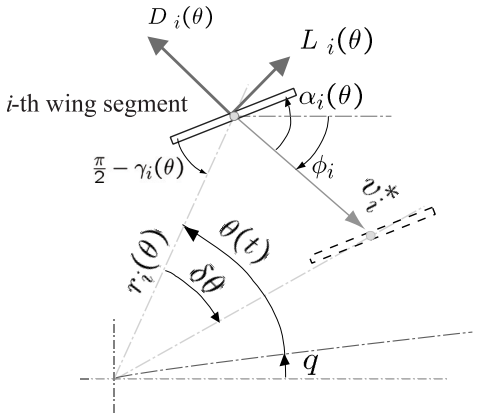

Fig. 5. Wing translation in i-th wing segment.

where $\delta\theta$ denotes a very small change of θ during the rotation and

$$\begin{aligned}\Delta\mathbf{R}_{c_h}(\theta) &= (\Delta R_{c_h x}(\theta), \Delta R_{c_h y}(\theta)) \\ &= \mathbf{R}_{c_h}(\theta + \delta\theta) - \mathbf{R}_{c_h}(\theta).\end{aligned}$$

The attack angle α can be calculated as

$$\alpha_i(\theta) = -\phi_i(\theta) + \theta + q + \gamma(\theta) - \frac{\pi}{2}. \quad (6)$$

For the velocity $v^*(\theta)$, the attack angle $\alpha_i(\theta)$ and the wing segment area $S = 2cb$, the lift and drag forces of wing segment i are given by

$$D_i(\theta) = \frac{1}{2}\rho v_i^{*2}(\theta) S C_D(\alpha_i(\theta)), \quad (7)$$

$$L_i(\theta) = \frac{1}{2}\rho v_i^{*2}(\theta) S C_L(\alpha_i(\theta)), \quad (8)$$

where $C_L(\alpha_i(\theta))$ and $C_D(\alpha_i(\theta))$ denote the lift and drag coefficients, respectively. The lift and drag coefficients at low Reynolds numbers ($Re = 10^4$) provided in [19] are used as $C_L(\alpha_i(\theta))$ and $C_D(\alpha_i(\theta))$, respectively.

Next, to calculate the total torque of n_f units with n wing segments, we define $r_i^*(\theta)$ as

$$r_i^*(\theta) = \frac{v_i^*(\theta)}{2\pi f} = \frac{1}{\delta\theta}\sqrt{\Delta R_{c_h x_i}^2(\theta) + \Delta R_{c_h y_i}^2(\theta)}. \quad (9)$$

The total torque $T(\theta)$ of n_f units with n wing segments is calculated as

$$T(\theta) = \sum_{i_f=1}^{n_f}\sum_{i=1}^{n}(D_i(\Theta_{i_f}) r_i^*(\Theta_{i_f})) + 2\pi C_{fric} f, \quad (10)$$

where

$$\Theta_{i_f} = \theta(t) + 2\pi\frac{i_f - 1}{n_f} \quad (11)$$

and C_{fric} is the friction loss coefficient of the prototype body given as $C_{fric} = 0.062$ [mNm·sec/rad] that is calculated from experimental data.

The motor power P can be expressed as

$$\begin{aligned} P(\theta) &= 2\pi T(\theta) f \\ &= 4\rho\pi^3 S \sum_{i_f}^{n_f} \sum_{i}^{n} \left(r_i^{*3}(\Theta_{i_f}) C_D(\alpha_i(\Theta_{i_f})) \right) f^3 \\ &\quad + 4\pi^2 C_{fric} f^2. \end{aligned} \tag{12}$$

Equation (12) shows the relation between $P(\theta)$ and f. Hence, for given $P(\theta)$, the rotational frequency f can be calculated by (12). Conversely, the power $P(\theta)$ can be obtained if the rotational frequency f is given.

The lift force $N(\theta)$ directing upward is calculated as

$$N(\theta) = \rho S C_N(\theta) f^2, \tag{13}$$

where

$$\begin{aligned} C_N(\theta) &= 2\pi^2 \sum_{i_f=1}^{n_f} \sum_{i=1}^{n} \{ r_i^{*2}(\Theta_{i_f}) C_D(\alpha_i(\Theta_{i_f})) cos\Theta_{i_f} \\ &\quad + C_L(\alpha_i(\Theta_{i_f})) sin\Theta_{i_f} \}. \end{aligned} \tag{14}$$

The total lift force N is obtained as

$$\begin{aligned} N &= \frac{1}{2\pi} \int_0^{2\pi} N(\theta) d\theta \\ &= \frac{1}{2\pi} \int_0^{2\pi} \rho S C_N(\theta) f^2 d\theta. \end{aligned} \tag{15}$$

C. Simulation and Experimental Results

Fig. 6 shows the simulation results for the fixed link's angle q and several rotational frequencies f at each revolving direction (CW or CCW), where CW and CCW denote clockwise and counter clockwise, respectively. It is found in the simulation results that the calculated lift forces are exactly the same in the CW and CCW directions and that there exists about 180 [deg.] phase difference with respect to q.

Table I is simulation results at the CCW and q=240 [deg.]. This results show that the robot can generate nearly 330 gf lift force exceeding its own weight (245 g). This shows the possibility of flying this mechanism.

TABLE I
SIMULATION RESULTS.

q=240 [deg.] and CCW			
Motor power P	40 W	50 W	60 W
Frequency f	7.9 Hz	8.6 Hz	9.2 Hz
Lift Force N	245 gf	290 gf	331 gf

Fig. 7 shows the experimental system for measuring lift forces. Lift forces are obtained by measuring strains of the aluminum bar with strain gages. Fig. 8 shows the experimental results of lift forces for q =40 [deg.] and q = 210 [deg.] at the revolving directions (CW and CCW). This results show that in spite of the same f, the lift forces are not the same for the revolving directions. The lift forces in the CCW direction are higher than those in the CW. In addition, the required power P in the CCW are higher than that in the CW as well. However these differences do not appear in the simulation results (Fig. 6) that indicates exactly the same force distributions. We will discuss a modification of the simulation model in the next section.

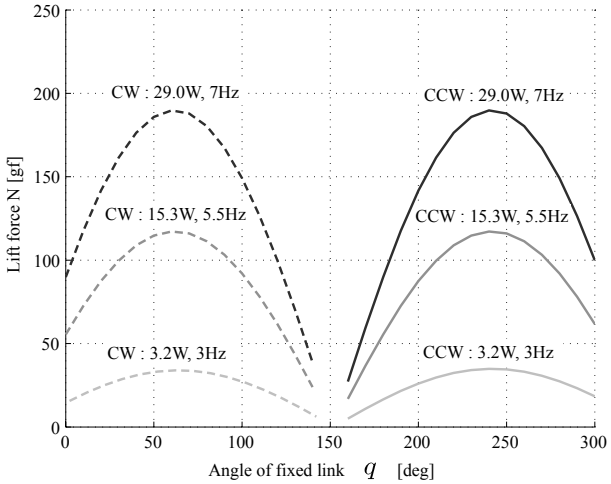

Fig. 6. Simulation results of lift forces for angle of fixed link.

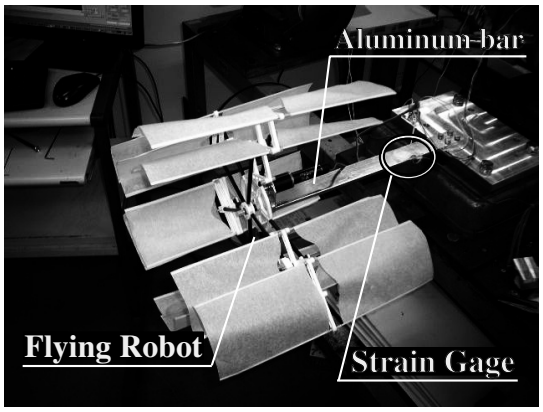

Fig. 7. Experimental system for measuring lift forces.

In Fig. 8, the highest lift force is generated at q=210 [deg.] in the CCW direction. Fig. 9 (a) (motor power P and frequency f) and (b) (frequency f and lift force N) show experiment results at q=210 [deg.] in the CCW. Table II shows a part of the experimental results given in Fig. 9 (a) and (b) at q=210 [deg.] in the CCW direction. The lift force arrives at 330 gf that is larger than its own weight (245 gf). This means that the generated lift force is sufficient to keep the robot in the air and the robot has 85 gf payload.

IV. NEW SIMULATION MODEL

As a reason of the simulation error between Figs. 6 and 8, we focus on a rotational effect of each wing. The simulation model considers only translational motions. The variable wing

TABLE II
PERFORMANCE AT EACH POWER AT q=210 [DEG.] IN CCW.

Motor power P	20 W	40W	60 W
Frequency f	6 Hz	7.8 Hz	9 Hz
Lift Force N	150 gf	235 gf	330 gf

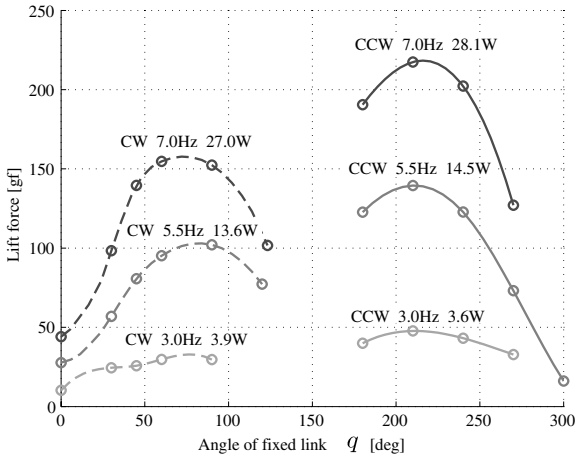

Fig. 8. Experiment results of lift forces for angle of fixed link.

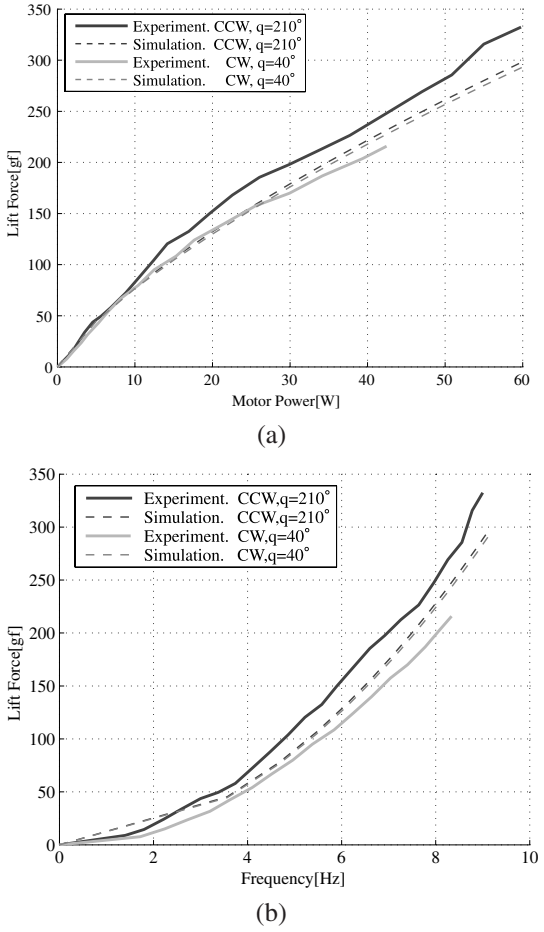

Fig. 9. Experiment result at q=210 [deg.] in CCW. (a) Motor power P and frequency f. (b) Frequency f and lift force N.

mechanism has a very remarkable flapping motion of the pantograph. As shown in Fig. 10, the force at highly rotating position contributes to upward in the CCW, whereas that at highly rotating position contributes to downward in the CW. Hence the rotational motion of the wings need to be considered for this mechanism.

In this section, we construct a new precise simulation model considering not only translational motions but also rotational motions. As a first step, we simply consider the individual force generated by rotational motion of each wing. The simulation results will show that even the simple consideration is effective to calculate lift force accuracy. As mentioned in Introduction, this paper focuses mainly on demonstrating the possibility of the flying robot with this mechanism. In near future, our focus will be shifted from demonstration of flying the robot (in experiment) to detailed aerodynamics analysis, e.g., [20–23]. The aerodynamics analysis for this remarkable wing motion is really interesting and will be one of next subjects in our research.

A. Rotational Wing Motion

Fig. 11 illustrates a wing rotation in the i-th wing segment. For the rotating velocity ω_{ri} and the translating velocity v_i^*, the leading edge velocity v_{i1} and the trailing edge velocity v_{i2} are expressed as

$$v_{i1} = v_{i1t}\mathbf{i}_v + v_{i1n}\mathbf{j}_v = \begin{bmatrix} v_i^* - c\omega_{ri}sin\alpha_i \\ c\omega_{ri}cos\alpha_i \end{bmatrix}^T \begin{bmatrix} \mathbf{i}_v \\ \mathbf{j}_v \end{bmatrix}, \quad (16)$$

$$v_{i2} = v_{i2t}\mathbf{i}_v + v_{i2n}\mathbf{j}_v = \begin{bmatrix} v_i^* + c\omega_{ri}sin\alpha_i \\ -c\omega_{ri}cos\alpha_i \end{bmatrix}^T \begin{bmatrix} \mathbf{i}_v \\ \mathbf{j}_v \end{bmatrix}, \quad (17)$$

respectively. According to conservation law of energy, pressure gradient ΔP is expressed as

$$\begin{aligned} \Delta P_i = P_{i1} - P_{i2} &= \frac{1}{2}\rho\big(|v_{i2}|^2 - |v_{i1}|^2\big) \\ &= \frac{1}{2}\rho({v_{i2}}_t^2 - {v_{i1}}_t^2) \\ &= \frac{1}{2}\rho(4c\omega_{ri}v_i^* sin\alpha_i). \end{aligned} \quad (18)$$

This means that ΔP is equal to the gradient of dynamical pressures of the wing velocity v_{i1t} and v_{i2t}. Hence assuming a flow and pressure field like water pressure illustrated in Fig. 12, the rotational lift F_{ri} of one wing segment is expressed as a pressure gradient force:

$$\begin{aligned} F_{ri} &= \begin{bmatrix} F_{ri_x} \\ F_{ri_y} \end{bmatrix} = \Delta P(2c\cos\alpha_i\ b)\mathbf{j}_v \\ &= \frac{1}{2}\rho(4c\omega_{ri}v_i^*\sin\alpha_i)(2c\cos\alpha_i\ b)\mathbf{j}_v \\ &= 4\rho c^2 b\omega_{ri}v_i^*\sin\alpha_i\cos\alpha_i \begin{bmatrix} -\sin\phi_i \\ \cos\phi_i \end{bmatrix}^T \begin{bmatrix} \mathbf{i}_x \\ \mathbf{i}_y \end{bmatrix}. \end{aligned} \quad (19)$$

Finally, the total upward (vertical-axis direction) force F_{ry} with respect to the rotational motion is calculated as

$$F_{ry} = \frac{1}{2\pi}\int_0^{2\pi} F_{ry}(\theta)d\theta, \quad (20)$$

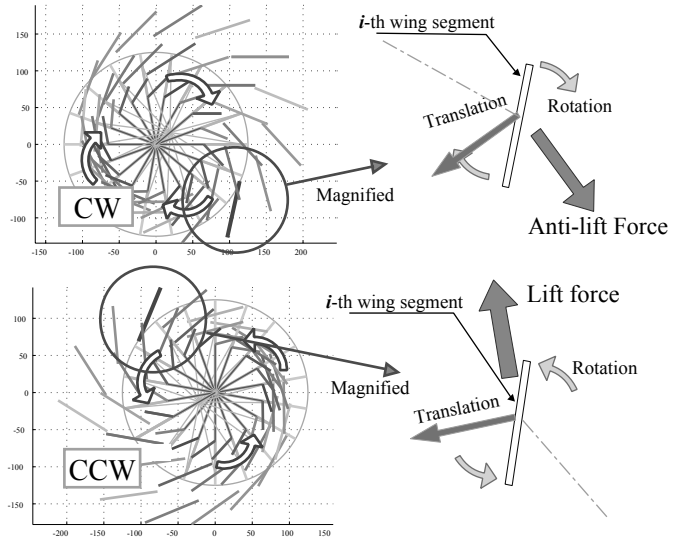

Fig. 10. Effect of rotating wing.

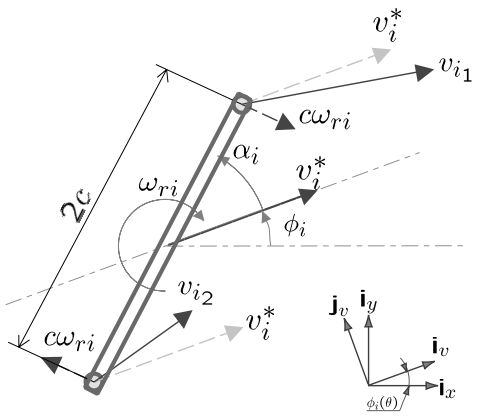

Fig. 11. Wing rotation in i-th wing segment.

where

$$\begin{aligned} F_{ry}(\theta) &= \sum_{i=1}^{n}\sum_{i_f=1}^{n_f} F_{ri_y} \\ &= 2\rho c^2 b \sum_{i=1}^{n}\sum_{i_f=1}^{n_f}\Big(\omega_{ri}(\Theta_{i_f}) v_i^*(\Theta_{i_f}) \\ &\quad \times \sin 2\alpha_i(\Theta_{i_f}) \cos\phi_i(\Theta_{i_f})\Big). \end{aligned} \tag{21}$$

B. Simulation Results

The total lift force N' considering the rotational motion can be calculated as $N' = N + F_{ry}$. Fig. 13 shows simulation results of lift force distribution N' for the angle of fixed link q with considering both translational and rotational effects. The results in Fig. 13 agree well with the experimental results in Fig. 8. Fig. 14 shows lift forces at each frequency (simulation and experiment). Thus, our developed simulation model considering the rotational motions has a sufficient high performance for calculating lift forces of the pantograph-based variable wing mechanism.

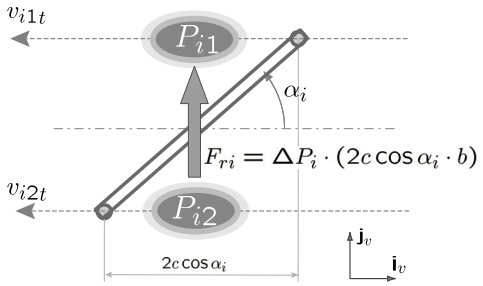

Fig. 12. Pressure gradient force F_{ri} in i-th wing segment.

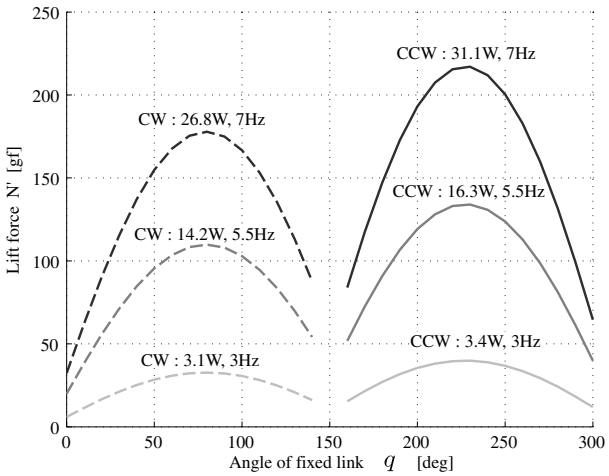

Fig. 13. Simulation results of lift force for angle of fixed link with consideration of rotational effect.

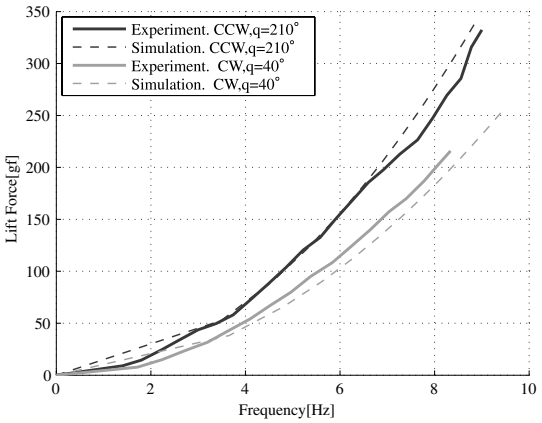

Fig. 14. Lift force at each frequency (simulation and experiment).

V. Redesign and Experimental Results

A. Optimal Design Parameters

In the previous section, we have showed the possibility of flying the developed prototype body. However flight performance of the robot with the optimal design parameters has not been considered. This section provides the optimization result for the design parameters of the robot through the simulation model developed in Section IV.

The purpose of the optimization is to determine the design parameters that can generate larger payload. To evaluate the

payload in the simulation model, we need to formulate a weight model $M[g]$ of the developed prototype body for changing the design parameters. By considering the specific gravity and sizes of materials, the weight model is formulated as

$$\begin{aligned} M &= 160 + 0.135(10+e) + 2.4n_f \\ &\quad +0.015(e+l-r_o+30+l)n_f \\ &\quad +5.7\times10^{-5}(r_o-20)^2 + 1.04\times10^{-5}(4n-3)n_f c^3 \\ &\quad +22S + 1.15\times10^{-7}b^3(n-1)n_f, \end{aligned} \tag{22}$$

where the first term is the weight of motor and all other unchanging structural parts, the second term is of fixed link, the third term is of sliders, the forth term is of cranks, the fifth term is of gears, the sixth term is of pantograph links, and the last two terms are of wings.

We search the optimal parameters by calculating the payload $P_L(= N' - M)$ for all combinations of variable parameters. In this paper we optimize the five parameters l, e, c, n_f and n, where the searching ranges are as follows:

$l = 80 \sim 140$ [mm], $e = 0 \sim 70$ [mm],
$n_f = 3 \sim 6$ [units], $c = 0 \sim 100$ [mm],
$n = 1 \sim 3$ [seg.].

Tables III and IV show optimization results for two cases of the motor powers (P=40 [W] and 60 [W]), respectively. In Tables III and IV, the payload of the prototype is also calculated through the simulation model. In particular, when the motor power is 60 [W], the optimal body can be expected to get over 165 gf payloads. This result means that the flying robot with the optimal parameters has 660 gf ($= 165 \times 4$) payload since the full model of the robot consists of four sets of the bodies as will be shown in Fig. 17.

TABLE III
OPTIMIZED DESIGN PARAMETERS I (40 W).

	n_f	n	l	e	c	$Payload$	$freq.$
	$units$	seg.	mm	mm	mm	gf	Hz
Optimized body	5	2	110	30	45	55	6.4
Prototype	5	2	100	25	40	16	7.7

TABLE IV
OPTIMIZED DESIGN PARAMETERS II (60 W).

	n_f	n	l	e	c	$Payload$	$freq.$
	$units$	seg.	mm	mm	mm	gf	Hz
Optimized body	5	2	110	30	45	165	7.4
Prototype	5	2	100	25	40	97	8.9

B. Experimantal Results

We build a flying robot with the optimal parameters given in Table IV. Fig. 15 shows the experimental system. The robot is put on the attachment. The attachment goes up and down along the vertical guide according to lift force generated by the robot. We need to provide the vertical guide so far since the robot can not be stabilized due to no feedback control. To investigate the lift force generated by the robot, the attachment with the robot is connected to the counter weight. The weights of the robot and the attachment are 248 g and 772 g, respectively. Even when the counter weight is 617 g, the robot can go up through the vertical guide. This result shows that the developed robot has at least 155 gf (= 772 - 617) payload. Fig. 16 shows flight performance experiment of the optimal body with the counter weight 617 g. The payload of the prototype mentioned in Section III is 85 gf. Hence, the design optimization achieves about 182 % flight performance improvement for the prototype. This result means that full body of the flying robot with the optimal parameters has 620 gf ($= 155 \times 4$) payload since the full body of the robot has four rotors as will be shown in Fig. 17. The power is supplied from outside in the current robot. However, this result shows that it is possible to fly the robot with a battery, some sensors and even a control board. A slight difference between the simulation result (165 gf lift force) and the experimental result (155 gf lift force) is mainly caused by the friction between the attachment and the vertical guide.

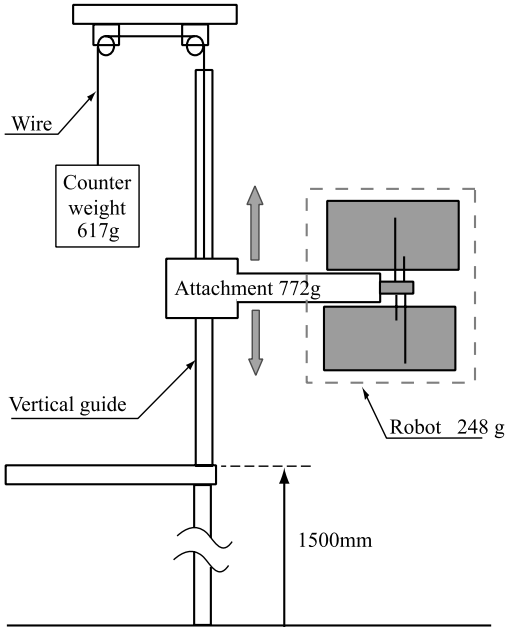

Fig. 15. Experimental setup.

VI. CONCLUSIONS

We have developed a flying robot with a new pantograph-based variable wing mechanism for horizontal-axis rotorcrafts (cyclogyro rotorcrafts). A key feature of the new mechanism is to have a unique trajectory of variable wings that not only change angles of attack but also expand and contract according to wing positions. We have presented some comparison results (between the simulation model and experimental data) for a prototype body with the proposed pantograph-based variable wing mechanism. Both simulation and experimental results show that the flying robot with this new mechanism can generate enough lift forces to keep itself in the air. Furthermore, we have constructed a more precise simulation model by considering rotational motion. As a result of optimizing

Fig. 16. Flight performance experiment.

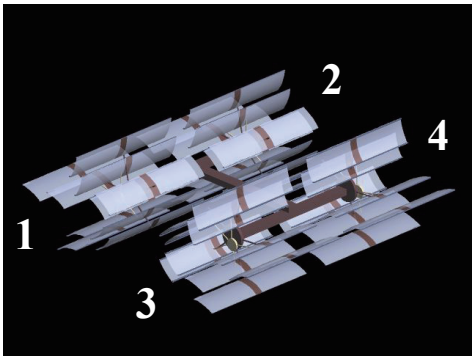

Fig. 17. Picture image of full model with four sets of developed bodies (pantograph-based variable wings).

design parameters using the precise simulation model, flight performance experimental results have demonstrated that the robot with the optimal design parameters can generate not only enough lift forces but also 155 gf payload.

Our next subjects are to consider detailed aerodynamics for this remarkable wing motion and to develop a full body flying robot with the optimal parameters. Fig. 17 shows images of the full model flying robot that we will develop. The full model consists of four sets of the bodies (pantograph-based variable wings) shown in Fig 4. The four pantograph-based variable wings are symmetrically located due to cancelling the total anti-torque generated by each pantograph-based variable wing. We will design a stabilizing controller for the robot using nonlinear control techniques.

REFERENCES

[1] Fritz-Olaf Lehmann, *The mechanisms of lift enhancement in insect flight*, Naturwissenschaften, vol.91, No.3, pp.101-122, 2004.

[2] M. H. Dickinson, F. O. Lehmann and S. P. Sane, *Wing Rotation and the Aerodynamic Basis of Insect Flight*, Science Vol.284, No.5422, pp.1954-1960, June 1999.

[3] R. S. Fearing, et. al., *Wing Transmission for a Micromechanical Flying Insect*, 2000 IEEE International Conference on Robotics and Automation, Vol.2, pp.1509-1516, San Francisco, CA, April, 2000.

[4] J.-C. Zufferey and D. Floreano, Fly-inspired visual steering of an ultralight indoor aircraft, IEEE Transactions on Robotics, Vol.22, No.1, pp.137-146, Feb. 2006.

[5] M. Abdulrahim and R. Lind, Modeling and control of micro air vehicles with biologically-inspired morphing, 2006 American Control Conference, pp.2718-2773, Minneapolis, June 2006

[6] S. Bermudez i Badia, P. Pyk and P.F.M.J. Verschure, A Biologically Based Flight Control System for a Blimp-based UAV, IEEE International Conference on Robotics and Automation, pp.3053-3059, Orlando, April 2005.

[7] H. Kobayashi, K. Kikuchi, K. Ochi and Y. Onogi, Navigation strategies referring to insect homing in flying robots, IEEE International Conference on Robotics and Automation, pp.1695-1700, Seoul, 2001

[8] K.D. Jones, C.J. Bradshaw, J. Papadopoulos, and M.F. Platzer,"Improved Performance and Control of Flapping-Wing Propelled Micro Air Vehicles" AIAA 42nd Aerospace Sciences Meeting and Exhibit, AIAA 2004-0399, Reno, Nevada, Jan., 2004

[9] J. M. Grasmeyer and M. T. Keennon, Development of the black widow micro air vehicle, AIAA Paper, No.2001-0127, pp.1-9, Anaheim, January 2001.

[10] S.M. Ettinger, M.C. Nechyba, P.G. Ifju, and M. Waszak, Vision-guided flight stability and control for micro air vehicles, 2002 IEEE/RSJ Int. Conference on Intelligent Robots and Systems, pp.2134-2140, Lausanne, Switzerland, October 2002.

[11] R.J. Wood, S. Avadhanula, E. Steltz, M. Seeman, J. Entwistle, A. Bachrach, G. Barrows, S. Sanders, and R.S. Fearing,"An Autonomous Palm-Sized Gliding Micro Air Vehicle: Design, Fabrication, and Results of a Fully Integrated Centimeter-Scale MAV ", IEEE Robotics and Automation Magazine, vol. 4, no. 2, pp. 82-91, June 2007.

[12] P. Samuel, J. Sirohi, F. Bohorquez, R. Couch, "Design and Testing of a Rotary Wing MAV with an Active Structure for Stability and Control", AHS 61st Annual Forum, Grapevine, TX, 1-3 June 2005.

[13] R.C. Michelson, "Novel Approaches to Miniature Flight Platforms, Proceedings of the Institute of Mechanical Engineers", Vol. 218 Part G: Journal of Aerospace Engineering, Special Issue Paper 2004, pp. 363-373, Dec. 2004.

[14] A. T. Conn, S. C. Burgess and C. S Ling, "Design of a parallel crank-rocker flapping mechanism for insect-inspired micro air vehicles", Proceedings of the Institution of Mechanical Engineers, Part C: Journal of Mechanical Engineering Science (Special Issue) 2007, vol. 221, no.10, pp.1211-1222, 2007

[15] T. Hase, *A cyclogyro-based flying robot*, SVBL conference in UEC, P-12, 2001

[16] T. Hase, T. Suzuki, K. Tanaka, T. Emaru, *A Flying Robot with Variable Attack Angle Mechanism*, The 21st Annual Conference of the Robotics Society of Japan, 3B22, in CD (2003)

[17] Y. Higashi, K. Tanaka, T. Emaru, and H. O. Wang, *Development of a Cyclogyro-based Flying Robot with Variable Attack Angle Mechanisms*, 2006 IEEE/RSJ International Conference on Intelligent Robotics and Systems, pp. 3261-3266, Beijing, 2006.

[18] The Cyclogyros:Planned paddle-wheel aeroplanes, http://www.dself.dsl.pipex.com/MUSEUM/TRANSPORT/cyclogyro/cyclogyro.htm

[19] I. Paraschivoiu, Aerodynamique subsonique, Presses internationales Polytechnique, Montreal, 1998.

[20] J. A. Walker, Rotational lift: something different or more of the same?, The Journal of Experimental Biology 205, pp.3783-3792, Dec. 2002

[21] M. H. Dickinson, F. -O. Lehmann and S. P. Sane, Wing rotation and the aerodynamic basis of insect flight, Sciences 284, pp.1954-1960, June, 1999

[22] J. A. Walker and M. W. Westneat, Mechanical performance of aquatic rowing and flying, Biological Sciences, Vol. 267, No. 1455, pp.1875-1881 , Sept. ,2000.

[23] M. Sun and J. Tang, Unsteady aerodynamic force generation by a model fruit fly wing in flapping motion, The Journal of Experimental Biology 205, pp.55-70, Jan. 2002.

Naohiro Hara received the B.S. degree in Department of Mechanical Engineering and Intelligent Systems from The University of Electro-Communications, Tokyo, Japan, in 2006.

Currently, he is a graduate student in Department of Mechanical Engineering and Intelligent Systems, The University of Electro-Communications, Tokyo, Japan. His research interests include developemnt and control of micro air vehicles.

Kazuo Tanaka (S'87 - M'91) received the B.S. and M.S. degrees in Electrical Engineering from Hosei University, Tokyo, Japan, in 1985 and 1987, and Ph.D. degree, in Systems Science from Tokyo Institute of Technology, in 1990, respectively.

He is currently a Professor in Department of Mechanical Engineering and Intelligent Systems at The University of Electro-Communications. He was a Visiting Scientist in Computer Science at the University of North Carolina at Chapel Hill in 1992 and 1993. He received the Best Young Researchers Award from the Japan Society for Fuzzy Theory and Systems in 1990, the Outstanding Papers Award at the 1990 Annual NAFIPS Meeting in Toronto, Canada, in 1990, the Outstanding Papers Award at the Joint Hungarian-Japanese Symposium on Fuzzy Systems and Applications in Budapest, Hungary, in 1991, the Best Young Researchers Award from the Japan Society for Mechanical Engineers in 1994, the Best Book Awards from the Japan Society for Fuzzy Theory and Systems in 1995, 1999 IFAC World Congress Best Poster Paper Prize in 1999, 2000 IEEE Transactions on Fuzzy Systems Outstanding Paper Award in 2000, the Best Paper Selection at 2005 American Control Conference in Portland, USA, in 2005.

He is currently serving on the IEEE Control Systems Society Conference Editorial Board. He is the author of two books and a co-author of 9 books. Recently, he co-authored (with Hua O. Wang) the book Fuzzy Control Systems Design and Analysis: A Linear Matrix Inequality Approach (Wiley-Interscience, 2001). His research interests include intelligent systems and control, nonlinear systems control, robotics and applications.

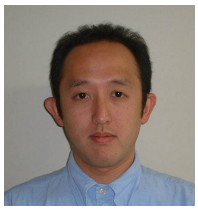

Hiroshi Ohake (S'02 - M'05) received the B.S. and M.S. degrees in mechanical and control engineering from The University of Electro-Communications, Tokyo, Japan, in 2000 and 2002, respectively. He is currently an Assistant Professor in Department of Mechanical Engineering and Intelligent Systems at The University of Electro-Communications, Tokyo, Japan He was a Research Fellow of the Japan Society for the Promotion of Science from 2002 to 2004. He received Outstanding Student Paper Award at the Joint 9th IFSA World Congress and 20th NAFIPS International Conference in Vancouver, Canada, in 2001, the Young Investigators Award from the Japan Society for Fuzzy Theory and Intelligent Informatics in 2003, the Best Presentation Award at the FAN Symposium 2004 in Kochi, Japan, in 2004, 2005 American Control Conference Best Paper Selection, at American Control Conference 2005 in Portland, USA, in 2005. His research interests include nonlinear mechanical systems control and robotics.

Hua O. Wang (M'94-SM'01) received the B.S. degree from the University of Science and Technology of China (USTC), Hefei, China, in 1987, the M.S. degree from the University of Kentucky, Lexington, KY, in 1989, and the Ph.D. degree from the University of Maryland, College Park, MD, in 1993, all in Electrical Engineering.

He has been with Boston University where he is currently an Associate Professor of Aerospace and Mechanical Engineering since September 2002. He was with the United Technologies Research Center, East Hartford, CT, from 1993 to 1996, and was a faculty member in the Department of Electrical and Computer Engineering at Duke University, Durham, NC, from 1996 to 2002. Dr. Wang served as the Program Manager (IPA) for Systems and Control with the U.S. Army Research Office (ARO) from August 2000 to August 2002. During 2000 - 2005, he also held the position of Cheung Kong Chair Professor and Director with the Center for Nonlinear and Complex Systems at Huazhong University of Science and Technology, Wuhan, China.

Dr. Wang is a recipient of the 1994 O. Hugo Schuck Best Paper Award of the American Automatic Control Council, the 14th IFAC World Congress Poster Paper Prize, the 2000 IEEE Transactions on Fuzzy Systems Outstanding Paper Award. His research interests include control of nonlinear dynamics, intelligent systems and control, networked control systems, robotics, cooperative control, and applications. He co-authored (with Kazuo Tanaka) the book Fuzzy Control Systems Design and Analysis: A Linear Matrix Inequality Approach (Wiley-Interscience, 2001). Dr. Wang has served as an Associate Editor for the IEEE Transactions on Automatic Control and was on the IEEE Control Systems Society Conference Editorial Board. He is an Editor for the Journal of Systems Science and Complexity. He is an appointed member of the 2006 Board of Governors of the IEEE Control Systems Society and a senior member of IEEE.